In situ measurements of explosive compound dissolution fluxes from exposed munition material in the Baltic Sea

Aaron J. Beck[1*], Eefke M. van der Lee[2], Anja Eggert[2], Beate Stamer[1], Martha Gledhill[1], Christian Schlosser[1], and Eric P. Achterberg[1]

[1] GEOMAR Helmholtz Centre for Ocean Research Kiel

[2] Leibniz-Institute for Baltic Sea Research Warnemünde

*Correspondence: ajbeck@geomar.de

Abstract

Underwater munitions containing millions of tons of toxic explosives are present worldwide in coastal marine waters as a result of unexploded ordnance and intentional dumping. Dissolution flux of solid explosives following corrosion of metal munition housings controls exposure of biological receptors to toxic munition compounds (MC; including TNT: 2,4,6-Trinitrotoluene, RDX: 1,3,5-Trinitro-1,3,5-triazinane, and DNB: 1,3-Dinitrobenzene). Very little is known about the dissolution behavior of MC in the marine environment. In this work, we exploit a unique marine study site in the Baltic Sea with exposed solid explosives to quantify in situ MC dissolution fluxes using dissolved MC gradients near the exposed explosive surface, as well as benthic chamber incubations. The gradient method gave dissolution fluxes that ranged between 0.001 and 3.2, 0.0001 and 0.04, and 0.003 and 1.7 mg cm^{-2} d^{-1} for TNT, RDX, and DNB, respectively. Benthic chamber incubations indicated dissolution fluxes of 0.0047-0.277, 0-0.11, and 0.00047-1.45 mg cm^{-2} d^{-1} for TNT, RDX, and DNB, respectively. In situ dissolution fluxes estimated in the current study were lower than most dissolution rates reported for laboratory experiments, but clearly demonstrated that MC are released from underwater munitions to the water column in the Baltic Sea.

TOC Art

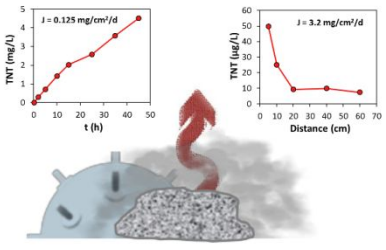

Introduction

Coastal marine environments are contaminated worldwide with millions of metric tons of dumped munitions and unexploded ordnance[1]. The majority of these underwater munitions were the result of activities during and after the World Wars (WW), especially WWII. As a consequence, coastal waters in Europe, North America, and the southwest Pacific are particularly heavily impacted. Records of munitions disposal are often incomplete or not sufficiently detailed, and the extent and type of munitions present in the coastal ocean is often not well known[2,3]. Underwater munitions represent a major hazard for development of offshore infrastructure such as aquaculture, wind farms, and oil or gas pipelines[4–6], increasing interest in removal and remediation of marine munitions.

In addition to the threat of detonation, many chemical compounds present in explosive materials are cytotoxic, genotoxic, and carcinogenic, and may represent an ecological hazard to marine organisms[7,8]. Undersea munitions may actually act as habitats for marine organisms[9,10], increasing the likelihood of food web exposure to munition related chemicals. Several studies have documented uptake of munitions compounds by organisms near underwater munitions[11–14]. These chemicals may enter the marine food web, and be present in seafood for human consumption[14], but the extent of this exposure is not known.

Dissolution of MC from explosive solids represents the initial controlling factor for release into the environment and exposure to ecological receptors. Reported dissolution rates increase rapidly with temperature, doubling with each 10°C increase [15,16]. A slight reduction of dissolution rate (<25%) has been reported for seawater (salinity 20) compared with fresh water[17]. Dissolution of MC from explosives solids also depends on formulation, with slowly soluble components such as HMX (1,3,5,7-Tetranitro-1,3,5,7-tetrazocane) tending to suppress the rate of more rapidly soluble components such as TNT (2,4,6-Trinitrotoluene)[16,18–20]. These effects on dissolution rate appear to be far outweighed by the effect of stirring or mixing speed, which results in rate variations over some three orders of magnitude[15,21]. In

terrestrial systems, simulations of dissolution by rainfall also show enhanced mass loss under higher flow conditions[22]. This suggests that dissolution rates under environmental conditions may not resemble those measured under ideal laboratory conditions.

Numerical oceanographic models can help to scale up dissolution rates to the water body and assess the environmental risk associated with dissolved MC. Some modeling efforts have been successful at describing the release of chemical constituents from breached munitions[23], but are nonetheless based on laboratory dissolution data (e.g., [24]). In order for oceanographic models to reliably simulate the transport and fate of these compounds in the water column, they must be based on kinetic parameters representative of munition compound dynamics in natural marine systems. Although MC dissolution is relatively well-constrained in freshwater under laboratory conditions, there are few data available in high ionic strength solutions or seawater[25,26], and no in situ measurements whatsoever. This represents a particular weakness in our ability to predict chemical release and spread in marine systems. The purpose of the current work was to exploit the unique presence of exposed munition material at a coastal study site to measure dissolution rates of MC under in situ conditions. To our knowledge, this is the first attempt to make such field measurements.

Materials and Methods

Site description and cruises

The Kolberger Heide munition dumping ground is located in the southwest Baltic Sea near Kiel, Germany, at approximately 54.4°N, and 10.3°E (Fig. S1). The site has brackish salinity (15-20), and a tidal range of less than 50 cm. Current speeds near the seafloor are slow, typically around 0.04 m/s and variable, but generally directed to the south-west. Bottom sediments are medium-coarse sands. The dumping ground is restricted to marine traffic, in an area of approximately 1,260 hectares and 10-15 m deep, located three to five nautical miles off the coast of Germany. The dumpsite was approved for munitions disposal in 1945, and is known to contain both German and British ordnance from World War II[14]. Some 30,000 tons of munitions are present at the site, and are thought to contain material comprising mainly TNT, RDX (1,3,5-Trinitro-1,3,5-triazinane), and DNB (1,3-Dinitrobenzene).

Within the Kolberger Heide site, there are clusters of munitions, such as a large pile of approximately 70 sea mines [27], but also more widely scattered ordnance such as ground mines, torpedoes, depth charges, and grenades. Some 6600 munition-like objects were identified on the seafloor during one survey of the 25 km^2 dumping ground[27]. Between 2009 and 2012, numerous large mines up to 550 kg in size were intentionally detonated at the site by military explosive ordnance disposal experts (EOD)[28,29]. In 2009, several of the mines underwent low-order detonation, which resulted in scattering of intact, exposed explosive material in the water column and on the seafloor[28]. Scientific divers at the site have observed large (meter-scale) piles of exposed explosives, as well as more wide-spread scattering of small pieces (few 10-30 cm diameter pieces per m^2). One piece of explosive material collected at the site was analyzed and found to be composed of TNT, ammonium nitrate, aluminum powder, and Hexyl (2,4,6-Trinitro-N-(2,4,6-trinitrophenyl)aniline)[30], while another was a combination of TNT, RDX, and Al powder (likely a formulation known as Torpex)[31]. After numerous dives at the study site, explosive ordnance

disposal (EOD) expert-trained research divers have noted that there are two visually distinct types of exposed munition material present: one is grey-silver in color (likely similar to the reported Torpex), and the other is orange-yellow in color (Fig. 1). The diversity of explosive sources at this study site (e.g., size of exposed surface, explosive formulation, ageing, biofouling) is likely to contribute to variability in the dissolution fluxes. It has unfortunately not been possible to further investigate the exact composition of the residual material due to safety concerns and legal restrictions on transport and possession of explosive material. Nonetheless, these exposed munition pieces provide a unique opportunity to study processes affecting mobility and fate of MC in the marine environment.

Sample collection and in situ experiments took place during three research cruises on *FK Littorina* in March, June, and October 2017 (denoted L17_03, L17_07, and L17_09, respectively). Water column characteristics (e.g., temperature, salinity) were measured by CTD (Sea & Sun Technology GmbH) to within approximately 2 m of the seafloor, but not deeper due to munition presence and safety concerns. Manual syringe sample collection and benthic chamber deployment were conducted by EOD-trained scientific divers from Christian-Albrechts-University, Kiel. These experiments were conducted as part of a project developing environmental impact assessment strategies related to future robotic munition removal approaches (UDEMM: Environmental monitoring for the delaboration of munitions on the seabed).

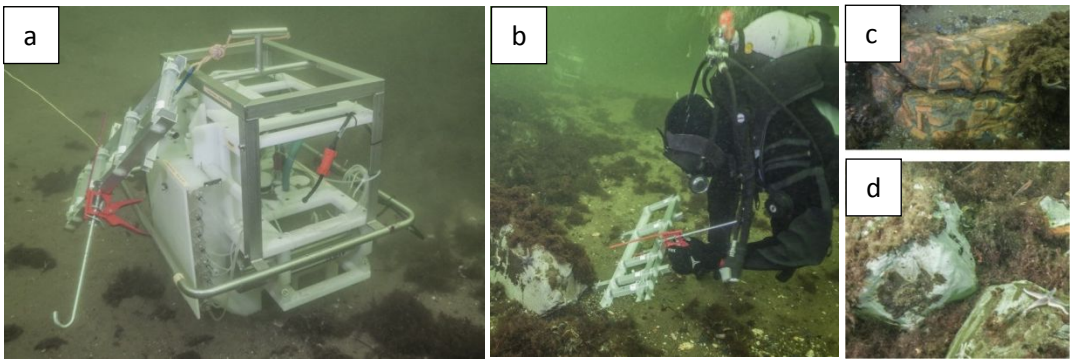

Figure 1. (a) Benthic chamber deployed on sandy bottom. The bank of glass syringes is visible on the left side, connected via tubing to the chamber in the center. The manual syringe sampler hangs off the handle to the left side. (b) Scientific diver preparing to collect a set of manual syringe samples adjacent to an exposed block of grey-silver explosive material. (c) Orange-yellow colored munition piece. (d) Grey-silver munition pieces. The scale in the latter two images is about 0.5 - 1 m. (Images: Forschungstauchzentrum CAU)

Syringe sampler (Gradient method)

The gradient method relies on samples collected manually by scientific divers at close intervals very near and vertical to the exposed munition surface. Because bottom currents at the study site are weak and variable (see Site Description), we assume that the direction of sampling did not greatly affect the profiles. The first set of syringe samples was collected during the March cruise using four individual 60 mL polypropylene syringes filled sequentially. We observed negligible adsorption of target analytes to plastic sampling materials within the short holding time (Supporting Information). In order to facilitate sampling and standardize the sampling distances during later sampling efforts, a device was custom-built that allowed simultaneous filling of five syringes at fixed positions 5, 10, 20, 40, and 60 cm from the munition surface (Fig. 1). Using this device, four sets of samples were collected during the June cruise, and six sets of samples were collected during the October cruise. The sets were collected on separate dives and on different munitions pieces. Most samples were collected near grey-silver pieces, but two sets purposely targeted the orange-yellow fragments.

Benthic chambers

Benthic flux chambers[32] (Fig. 1) were adapted in this study for measuring dissolution of solid munition pieces by emplacement over exposed fragments of explosive material resting on the flat sandy seafloor. Chambers were cylindrical polycarbonate enclosures 19 cm in diameter, and contained about 9 L of

water after insertion ~5 cm deep into the sediment. Water within the chamber was mixed very gently by a small rotor in the chamber lid. After deployment and a delay period, the chamber was flushed with ambient water for 30 minutes by an impeller pump. Samples were collected automatically at predetermined intervals (0.2 – 10 h) with 60 mL glass syringes connected to the chamber by Vygon tubing. Dissolved oxygen was monitored inside and outside the chamber by two optodes (ANDERAA) to evaluate if sediment enclosure in the chambers affected redox conditions.

Two separate benthic chambers were deployed during both March and October cruises. In March, one chamber failed to operate and the other collected samples only during the first 15 hours, but both chambers worked for the entire 48h deployment in October (although data from one chamber could only be used before the 25h time point, see below). During the March deployment (L17_03), the benthic chamber was placed over an orange-yellow munition piece that was approximately 5x6x4 cm (118 cm^2, not including the face lying on the sediment). In October (L17_09), both pieces were grey-silver colored and approximately 6 cm on all sides (180 cm^2).

Chemical analysis

After collection, water samples were transferred to 50 mL polypropylene centrifuge tubes, stored at 4 °C, and processed within 24 h. Dissolved MC were measured by ultra high performance liquid chromatography-electrospray ionization mass spectrometry (uHPLC-ESI-MS)[33]. Briefly, all samples were initially diluted 100-fold with 50% LCMS-grade methanol and measured following direct injection. Samples with concentrations below approximately 1 µg L^{-1} were preconcentrated on Chromabond Easy resin columns, eluted with LCMS-grade acetonitrile, brought to near dryness, and reconstituted in 50% LCMS-grade methanol. Samples were then measured as for direct injection. Detection limits of this method are on the order of 0.01 µg L^{-1} for the analytes of interest.

Turbulent or eddy diffusion coefficients

Turbulent mixing drives water exchange near submerged explosive surfaces, and therefore is a dominant control on mass transfer and dissolution. Eddy diffusion coefficients (K_v) were estimated using two independent approaches based on (1) calculation using velocity profiles in the water column, and (2) eddy-diffusion values extracted from an eddy-resolving hydrodynamic model, the General Estuarine Transport Model (GETM). Under normal conditions, the turbulence structure could be very highly resolved using a Microstructure Probe, but it is unfortunately not possible to use a free-falling instrument in a munitions-contaminated site due to explosion risk. An Acoustic Doppler Current Profiler (ADCP) was deployed at the sea bed almost continuously throughout 2017. The ADCP recorded water current velocity and direction every 15 minutes in bins of 25 cm height from 1.3 m above the bed up to the water surface. Current velocity profiles were time-averaged (following [34]), and the resulting profile used to estimate the eddy diffusion coefficient. Averages were calculated over the cruise sampling periods in June and October, representing 208 and 128 individual profiles, respectively. For the March cruise, velocity data was not available for the exact sampling date (16 March), hence the first available date afterwards (30 March) was used (66 individual velocity profiles).

For this study, we used a western Baltic Sea configuration of the hydrodynamic model GETM with a horizontal resolution of 1/3 nautical mile (approx. 600 m). The model domain covers the Danish Straits and the western Baltic. The model setup uses realistic atmospheric forcing derived from the operational model of the German Weather Service (DWD) with a spatial resolution of 7 km and temporal resolution of 3 h. In the vertical we used 42 terrain-following adaptive layers, with a minimum layer thickness of 0.3 m. The present setup is identical to the one used by [35] and a detailed description and validation of the used setup is given in [36] and [37]. Results from the GETM model for 2017 were not available, so eddy diffusion values were taken from the 2016 model run. Values were calculated every 30 minutes between Jan 1 and Oct 31, for the vertical bin closest to the seafloor. Although both methods required compromises in terms of data availability and timing, the objective here was to constrain a

representative eddy diffusion value for the site. Fine scale variability in K_v may exist within the site or over short time scales, and this adds an additional degree of uncertainty to the dissolution flux estimates.

Results

Water column chemistry

Water column profiles of salinity and temperature showed weak stratification approximately 4-5 m above the seafloor, with a well-mixed layer above (Supporting information, Fig. S2). Water temperature was lowest in March (3.3 – 3.9°C), and salinity was highest (16.1 – 18.2). In June, water temperature was highest (15.4 – 16.5°C) and salinity intermediate (16.7 – 17.5). In October, stratification was weakest, with intermediate salinity (15.4 – 16.5 ppt) and the narrowest range in water temperature (13.5 – 13.6°C). Dissolved oxygen and pH (NBS scale) were only measured during the October cruise, and ranged between 240 and 320 µM, and 7.5 and 7.9, respectively. Bottom waters were around 85% oxygen saturation.

Manual syringe samples

Syringe samples were collected along a 50 cm long transect with individual syringes in March. Because individual syringes were used, the first sample was collected directly at the munition surface (i.e., at 0 cm from the solid surface). Dissolved TNT in this sample was 3100 µg L^{-1} (Fig. 2), the highest observed in any manual syringe sample. Concentrations declined rapidly away from the munition surface, to 16 µg L^{-1} at 1 cm and finally 3.3 µg L^{-1} at 50 cm distance. Dissolved RDX and DNB showed a similar trend, but the concentrations were lower (~1 – 10 µg L^{-1}). Samples collected during the June and October cruises showed less striking decreases (maximum measured TNT was 50 µg L^{-1}), likely because the simultaneous

199 syringe sampling device collected the first sample at 5 cm distance from the munition surface. Indeed,
200 the trends and concentrations in March match the other sampling periods when distances 1 cm and
201 greater are considered. Most samples from these later cruises showed monotonous declines in TNT away
202 from the munition surface, although three sets did not show elevated levels in the near-surface sample
203 (distance = 5 cm). The lowest concentrations were consistently observed for RDX, generally 1-2 μg L^{-1} or
204 less, and profiles often did not show a clear decreasing trend away from the surface. Trends were also
205 less clear for DNB, although concentrations were as high 22 μg L^{-1}.

206 Most syringe sample sets were collected near grey-silver colored munition pieces, although two sets
207 collected in October intentionally targeted the orange-yellow colored pieces. Trends for TNT in these
208 sample sets were not markedly different from those collected on the grey-silver pieces, with
209 concentrations nearest the surface of 22-23 μg L^{-1}. No obvious difference was apparent for RDX or TNB
210 either; highest measured concentrations of DNB were measured in the samples from the orange-yellow
211 pieces, but the data were scattered and not substantially different from the other sample sets.

212 *Benthic chambers*

213 Benthic chambers were deployed twice, once in March (Chamber 1), and once in October (Chamber 2
214 and 3). Oxygen levels in the chambers declined slightly during the incubation, by between 15 and 25%, to
215 291 μM in March and 238 μM in October (data not shown). The oxygen levels measured within
216 chambers in October were only slightly lower at the end of the incubation period than in the water
217 column, indicating that redox conditions within the chambers were not greatly altered during the
218 incubation.

219 During the March cruise, one chamber failed to operate, and the second stopped collecting samples after
220 15 hours. Nonetheless, the retrieved samples showed an increase in concentration within the chamber
221 ("Chamber 1", Fig. 3). During this deployment, the chamber was placed over an orange-yellow munition

piece. Very little TNT dissolution was observed in this chamber (maximum 58 μg L^{-1}, after 15 h), although RDX concentrations reached 920 μg L^{-1} after 15 h. In contrast, DNB reached levels of 11300 μg L^{-1}. The temporal trend was similar for RDX and DNB.

In October, two chambers were deployed successfully (Fig. 3). In Chamber 2, dissolved TNT and DNB increased monotonously, reaching concentrations of 4500 and 17.8 μg L^{-1}, respectively. RDX increased very slightly to less than 1 μg L^{-1} over the 48 h incubation period. In Chamber 3, TNT and DNB increased over the first five time points to 3410 and 46.2 μg L^{-1}, respectively. RDX was not detected in the chamber over this period. Between 15 and 25 h, concentrations of TNT and DNB decreased to ambient levels (<1 μg L^{-1}). This was most likely caused by the chamber tilting and allowing ambient water to enter under the chamber lip. Oxygen data in the chamber confirm this, with a slow decline in dissolved oxygen initially that returned to ambient conditions and matched oxygen trends outside the chamber thereafter (data not shown). Because of the sandy sediments in the study region, divers were unable to insert the chamber mouth very deep, making them rather physically unstable. Regardless, the initial time points appear to have provided reliable data.

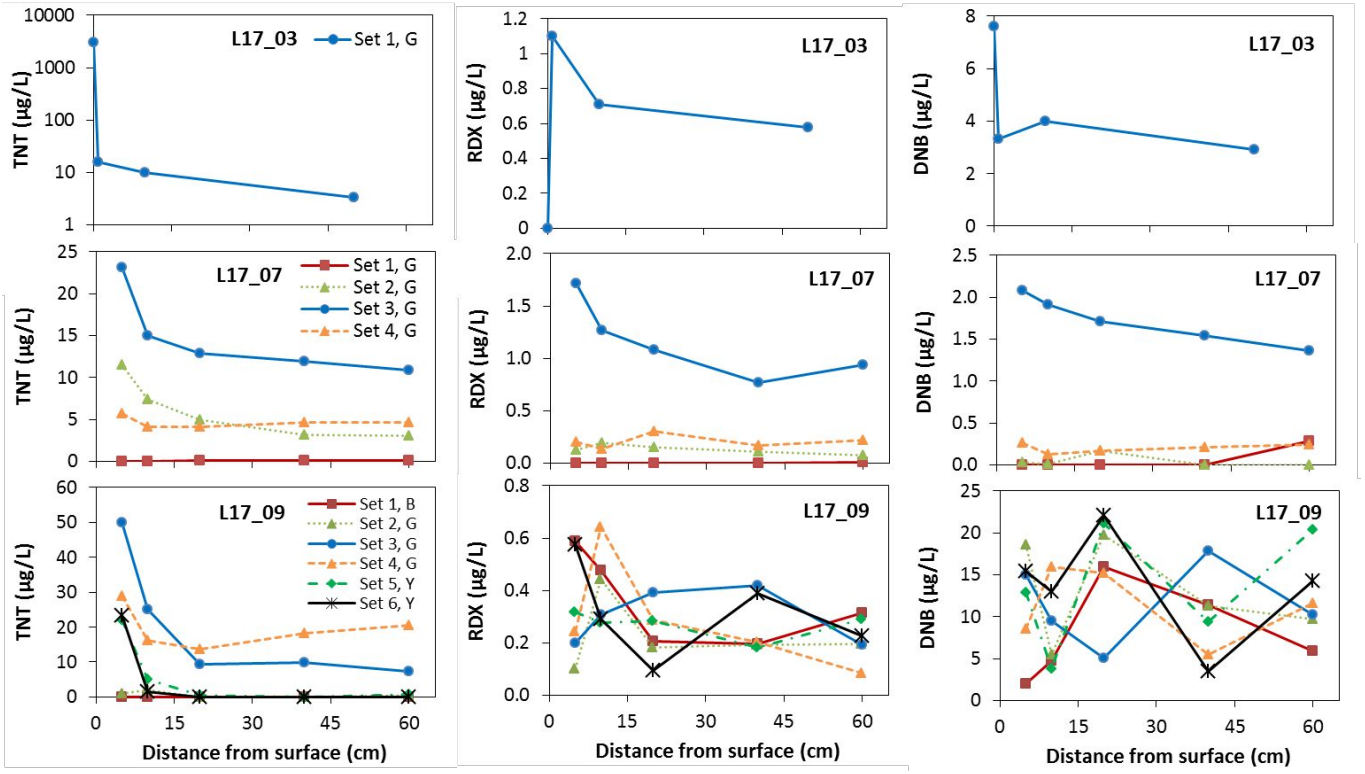

Figure 2. Manual syringe sample sets during three sampling cruises. L17_03: March 2017, L17_07: June 2017, L17_09: October 2017. Each set of syringe samples was collected on a different exposed munition piece; letters indicate type: "G" is grey/silver colored, "Y" is orange-yellow colored, and "B" is unknown. Note the log scale concentrations for L17_03 TNT. Replicate samples could not be obtained with the sampling device, and uncertainties associated with the ~5% analytical precision are omitted for clarity.

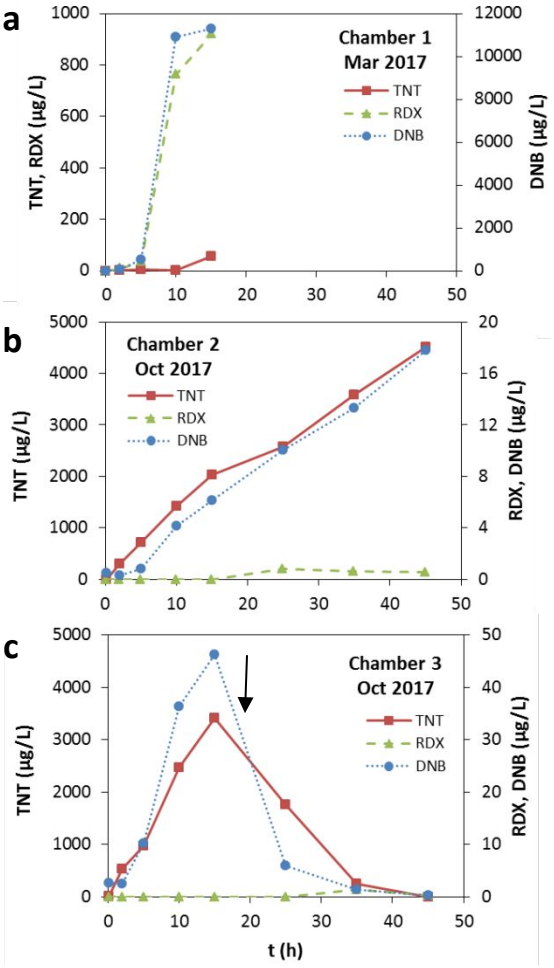

Figure 3. Time series of MC concentrations measured in benthic chambers (18 L volume). a) March 2017. Syringe sampler failed mid-deployment, limiting the incubation time. b) October 2017, ideal deployment. c) October 2017, replicate chamber. Concentrations declined between 15 and 25h (black arrow), likely due to the chamber tilting and venting to surrounding water. Chamber 1 was placed over a yellow-orange munition piece, whereas Chambers 2 and 3 were placed over grey-silver pieces. Replicate samples could not be obtained with the sampling device, and uncertainties associated with the ~5% analytical precision are omitted for clarity.

Eddy diffusion coefficient, K_v

The velocity profiles generally adhered to the "law-of-the-wall" distribution[38]—i.e., exhibiting a logarithmic profile close to the seabed "wall" (Fig. S3). The mean velocity, *U(z)*, can therefore be described as a function of depth according to:

$$U(z) = \left(\frac{u_*}{k}\right) ln\left(\frac{z}{z_0}\right) \quad \text{Equation 1}$$

where u_* is the friction velocity, k is the dimensionless von Kármán constant with a value of 0.41, z is the height above the sea bed, and z_0 is the bottom roughness height. For each of the data periods, a mean velocity profile was calculated from the measured profiles (Fig. S3). In a plot of *U(z)* against *ln(z)*, u_* is the slope of the straight line fit for the bottom region multiplied by k. The height above the bed at which the velocity is zero and the logarithmic profile starts (z_0), can be calculated from this fit as well at the point z = 1, i.e., ln(z) = 0, by re-arranging Eq. 1 to:

$$z_0 = e^{U_{z=1}\, k/u_*} \quad \text{Equation 2}$$

In this case, the deepest 15 bins were used, corresponding to bin mid-depths from 1.3 to 4.8 meters above the sea bed. During the sampling periods, u_* was estimated as 6.4±0.5 mm s^{-1} (June), 6.0±0.6 mm s^{-1} (March), and 1.3±0.8 mm s^{-1} (October), with a z_0 average of 6.6 cm.

With u_*, we can calculate the near-bottom vertical eddy diffusion coefficient, K_v, which is given by[38]:

$$K_v = k u_* z \quad \text{Equation 3}$$

Accordingly, the value of K_v increases linearly with height from 0 m^2s^{-1} at the sea bed. At a 10 cm sampling depth for the syringe profiles, the mean K_v was (2.5±0.2)×10^{-4}, (2.6±0.2)×10^{-4}, and (0.5±0.3)×10^{-4} m^2s^{-1} , for March, June, and October, respectively. Uncertainty on these K_v values is propagated from the error of the linear regression used to estimate u_*.

As an independent approach for estimating the eddy diffusion coefficients (to improve confidence in the dissolution rate calculations), values were also taken from the GETM circulation model. In general, bottom water eddy diffusivities were higher during the stormier winter months, but there is a high degree of variability over the period January to November 2016 (Fig. S4). Model results were not available for 2017, so results for 2016 were substituted. Average values for March, June, and October were $(0.8\pm2.1)\times10^{-4}$, $(0.2\pm0.7)\times10^{-4}$, and $(0.6\pm10)\times10^{-4}$ m^2s^{-1}. Thus, model-derived values of K_v are more variable than the velocity profile approach, but match within the uncertainty.

The average eddy diffusivity of these two approaches across the sampling periods is $(1.2 \pm 1.1)\times10^{-4}$ m^2s^{-1} (avg. ± 1 s.d.), consistent with previous work showing order-of-magnitude increases in the average eddy diffusivity in the Baltic Sea from interior basins (~10^{-6} m^2s^{-1}), to entire basin (~10^{-5} m^2s^{-1}), to basin margins [39]. For the purpose of the current work, we use the average value of 1.2×10^{-4} m^2s^{-1}, although estimated dissolution fluxes would change correspondingly if the actual diffusivities were higher or lower. Further measurements with microstructure profilers, and sampling of MC gradients with higher temporal resolution would be required to determine how well assumptions of steady state are met in this system.

Discussion

Dissolution fluxes by the gradient method

The syringe sample datasets generally showed elevated levels near the munitions surface, with a decline towards the overlying water column. This trend suggests that MC are released to the water column by dissolution of the solids, and mixing processes rapidly dilute the concentrations within 60 cm of the munition surface. This is consistent with MC gradients observed by Rosen and colleagues[40] in an experiment using passive samplers and an explosive point source. Degradation is unlikely to contribute

295 to the decrease given that MC half-lives in the marine environment are on the order of days to weeks ([41],
296 and references therein).

297 A simple steady state model can be devised under which the dissolution rate at the munition surface
298 (J_{dissol}) is equal to the flux of dissolved MC from the solid material (J_{MC}) controlled by eddy diffusion. The
299 flux is proportional to the product of the eddy diffusion coefficient (K_v), the area normal to the source,
300 and the concentration gradient away from the surface[42]. For radial diffusion from an explosive piece on
301 the seafloor, the area normal to the source at distance *r* from the center of the half sphere is $2\pi r^2$, *SA* is
302 the explosive surface area, and the MC concentration gradient is dC_{MC}/dr:

303 $$J_{dissol} = J_{MC} = -K_v\left(\frac{2\pi r^2}{SA}\right)\frac{dC_{MC}}{dr}$$ Equation 4

304 The eddy diffusion coefficient is estimated using the velocity profiles and GETM model results, and the
305 concentration gradient is calculated from the two samples in each syringe set closest to the munition
306 surface (*r* = 10 cm; Table 1). For the sample set from cruise L17_03, the concentration gradient was
307 estimated using samples at 1 and 10 cm (omitting the high concentration measured directly at the
308 explosive surface). Turbulent diffusion decreases rapidly near to the solid surface, so the first sample
309 therefore overestimates the concentration gradient corresponding to the applied eddy diffusion
310 coefficient, and gives a flux estimate that is unrealistically high. To make this first sample set consistent
311 with the others, only data from distances >1 cm were used to estimate the gradient.

312 The point source is assumed to have a surface area of 100 cm^2, similar to the explosive pieces used in
313 benthic chamber deployments (below), although many explosive pieces at the site are larger (e.g., Fig. 1).
314 As the area of the exposed surface increases, the source becomes more laterally uniform, and a 1-
315 dimensional model is more appropriate (i.e., eliminating the $2\pi r^2/SA$ term from Eq. 4, and decreasing the
316 flux estimate). Thus, the fluxes estimated here probably represent the maximum values for this site.

317 Dissolution fluxes estimated using this approach were consistent among the different sample sets (Table
318 1). For TNT and DNB, dissolution fluxes were generally on the order of 10^{-1}-10^{0} mg cm^{-2} d^{-1}, and RDX
319 dissolution on the order of 10^{-2}-10^{-1} mg cm^{-2} d^{-1}.

Table 1. Dissolved MC gradients near munitions surfaces, and calculated dissolution fluxes (where K_v = 1.2×10^{-4} m^{2}s^{-1}). Letters in the sample ID refer to the apparent munition type, as described in the Methods section: "G" is grey-silver, "Y" is orange-yellow, and "B" is unknown.

		dC/dr (ng cm^{-3} cm^{-1})			**J_{dissol} (mg cm^{-2} d^{-1})**		
		TNT	**RDX**	**DNB**	**TNT**	**RDX**	**DNB**
L17_03*	Set 1, G	0.67	0.043	--	0.4	0.03	--
L17_07	Set 1, G	0.002	0.0001	--	0.001	0.0001	--
	Set 2, G	0.83	--	0.005	0.5	--	0.003
	Set 3, G	1.6	0.090	0.036	1.1	0.1	0.02
	Set 4, G	0.32	0.013	0.027	0.2	0.01	0.02
L17_09	Set 1, B	0	0.022	--	0	0.01	--
	Set 2, G	--	--	2.6	--	--	1.7
	Set 3, G	4.9	--	1.1	3.2	--	0.7
	Set 4, G	2.5	--	--	1.6	--	--
	Set 5, Y	3.4	0.008	1.8	2.2	0.01	1.2
	Set 6, Y	4.4	0.057	0.47	2.8	0.04	0.3
Average		1.9 ± 1.8	0.033 ± 0.032	0.87 ± 1.0	1.2 ± 1.2	0.022 ± 0.021	0.57 ± 0.67

*For L17_03, the concentration gradient is estimated using samples between 1 and 10 cm distance (see text).

Estimates are omitted where gradients increase away from the munition surface.

Uncertainties on individual estimates are not available because each sample profile represents a single set of unreplicated samples. The standard deviation of the average gives the best indication of uncertainty on these estimates.

Dissolution fluxes in benthic chambers

Dissolution fluxes were calculated in benthic chamber experiments by fitting linear regression trendlines (intercept at the origin) to the incubation data, giving the rate, R (μg L^{-1} d^{-1}), of concentration increase as a function of time. Fluxes were then calculated using the exposed surface area of the enclosed munition pieces (A; cm^2), and the volume of the chamber (V; L):

$$J_{chamber} = \frac{R \times V}{A} \qquad \text{Equation 5}$$

All data were used in Chambers 1 and 2; in Chamber 3, only data from the first 15 hours were considered (Table 2). A striking difference in MC dissolution was observed between the orange-yellow munition piece (Chamber 1) and the grey-silver pieces (Chambers 2 and 3) (Fig. 3). Concentrations of DNB and RDX increased greatly in Chamber 1, suggesting that these two compounds make up a major portion of the orange-yellow munition solids. Dissolution fluxes of DNB and RDX in Chamber 1 were similar to the gradient samples. In contrast, TNT dissolution in Chamber 1 was slower than any of the estimates made by the gradient method. Given the apparent DNB/RDX composition of the orange-yellow solids, it is surprising that neither of these compounds were visibly elevated in syringe samples collected near orange-yellow pieces (Fig. 2). This is probably either because the chemical composition is in fact not related to the color, or there is substantial heterogeneity in the chemical emission from the solids and syringe sampling inadvertently missed the plume.

Table 2. Dissolution fluxes obtained from benthic chamber incubations.

	Dissolution rate (mg cm^{-2} d^{-1})		
	TNT	**RDX**	**DNB**
Chamber 1 [a]	$(4.7 \pm 1.6) \times 10^{-3}$	0.11 ± 0.016	1.45 ± 0.24
Chamber 2 [a]	0.125 ± 0.005	$(1.8 \pm 0.4) \times 10^{-5}$	$(4.7 \pm 0.1) \times 10^{-4}$
Chamber 3 [b]	0.277 ± 0.008	0	$(3.8 \pm 0.3) \times 10^{-3}$

[a] Calculated using all data

[b] Calculated using data from 0-15 h

Uncertainties are calculated from the error on the regression used to derive the rate of concentration increase in the chambers with time (*R*, Eq. 5)

339

340 In Chambers 2 and 3, little RDX dissolution was evident, but both TNT and DNB showed substantial
341 dissolution (Fig. 3). The increasing concentration trend was identical for TNT and DNB in both chambers,
342 but TNT reached levels that were approximately 100-fold higher than DNB. Dissolved TNT concentrations
343 in the chambers reached approximately 4 mg L^{-1}, which is about 5-10% of the saturation limit (~50-80 mg
344 L^{-1} at 3-15°C; see compilation in [41]). This is consistent with previous studies showing very high
345 concentrations of MC within cavities of breached munitions[12], and suggests a high level of heterogeneity
346 in MC concentration within munitions-contaminated sites, depending on frequency and intensity of
347 water exchange.

348 Dissolution fluxes for TNT, RDX, and DNB in the benthic chambers were between approximately 10^{-4} and
349 10^{-1} mg cm^{-2} d^{-1} (Table2). Chamber fluxes matched well with those estimated from the gradient samples
350 for TNT in Chambers 2 and 3, whereas RDX and DNB fluxes in Chamber 1 matched the gradient-method
351 estimates better. Little RDX and DNB dissolution was observed in Chambers 2 and 3, and estimated
352 fluxes were several orders of magnitude lower than estimated from the syringe sample gradients. These
353 differences most likely reflect the high degree of variability in the munitions present in marine
354 dumpsites. There are many formulations with different nominal compositions (e.g., Filling 84: 100% DNB
355 vs. Filling 96: 50% each TNT and RDX); there are more than 430 different German explosive mixtures[43],
356 and actual formulations likely varied from the nominal composition during wartime due to ingredient
357 availability.

358 Table 3. Comparison of dissolution fluxes measured in the current work with those reported from previous studies in fresh and brackish water.

Solvent	Explosive formulation	Dissolution rate (mg cm^{-2} d^{-1})			Notes	Reference
		TNT	RDX	DNB		
Seawater (15-18 ppt)	Unknown	0.0047 - 0.277	0.000018 - 0.11	0.00047 - 1.45	Benthic chamber incubation	This work
Distilled water	Octol	0.072	n.m.	n.a.	25°C, no stirring.	[21]
Rainwater	Comp B	0.329	0.324	n.a.	Column experiment, 10 cm/d flow	[44]
Rainwater	C4	n.a.	0.674	n.a.	Column experiment, 10 cm/d flow	[44]
Seawater (15-18 ppt)	Unknown	0.001 – 3.2	0.0001 – 0.04	0.003 – 1.7	Open water gradient method	This work
Deionized water	Comp B	5.6	1.7	n.a.	Stirred, 150 rpm	[17]
Sea water (20 ppt)	Comp B	5.6	1.9	n.a.	Stirred, 150 rpm	[17]
Deionized water	Octol	11	n.m.	n.a.	Stirred, 150 rpm	[17]
Sea water (20 ppt)	Octol	10	n.m.	n.a.	Stirred, 150 rpm	[17]
Sea water (20 ppt)	Pure solid	13	n.m.	n.a.	Stirred, 150 rpm	[17]
Deionized water	Octol, GIM	12 - 28	n.m.	n.a.	Stirred, 300 rpm	[19]
Deionized water	Pure solid	18	n.m.	n.a.	Stirred, 150 rpm	[17]
Deionized water	Pure solid	70 - 76	1.2 - 8.4	n.a.	Stirred, 90-210 rpm, 10-30°C	[15,45]
Deionized water	Comp B	74	40	n.a.	Shaker table at 225 rpm	[46]
Unknown	Unknown	100	8.64	n.a.	"Completely stirred"	[25]

n.a. - Not Applicable

n.m. - Not Measured

Comparison with previous studies and implications

The dissolution fluxes determined in the current work show large variability, but are similar to the lower laboratory measurements reported in the literature (Table 3). Dissolution fluxes measured with the benthic chambers match the lowest reported fluxes for TNT and RDX. The gradient method estimates are similar to the lowest reported fluxes for TNT, whereas estimates for RDX are lower than literature values by 100-fold or more. We are not aware of any previous measurements of DNB dissolution fluxes, but the estimates here are similar to TNT and RDX.

There is large variability in the dissolution rates estimated in the current study, but they are nonetheless lower by orders-of-magnitude than most of the rates reported in the literature. It is possible that the eddy diffusion coefficients applied here were too low (note, for example, the GETM model estimates in Fig. S4 show large variability around the mean), which would underestimate the true flux. In addition, we were unable to measure the exact composition of the dissolving source material, so it remains unknown how well the aged explosive material present in Kolberger Heide can be compared with formulations used in previous laboratory experiments.

We believe instead that the difference between our in situ rates and those from previous laboratory studies results from the degree of stirring or mixing during the experiment. The benthic chamber results match best with column experiments with very slow flow[44] or batch experiments with no stirring[21]. The gradient method estimates match better with experiments under slightly higher stirring speeds, suggesting control by rapid water mixing in shallow coastal waters. Dissolution fluxes estimated with the gradient method were similar for different sampling cruises, suggesting that temperature differences had little effect on dissolution, despite variations of 3-16°C. Estimates in the current study are similar to literature values for both fresh and higher salinity water, suggesting that a salinity effect on dissolution is likely small relative to other factors. It is therefore likely that dissolution of exposed munitions on the

seafloor and release of MC to the water column is limited in low-energy marine systems, such as deep waters. However, in shallow coastal systems, tides, wind, and waves may greatly enhance water mixing around objects on the seafloor, and increase the rate of MC release from underwater munitions. Storm events may also lead to episodic pulses of MC release.

From the MC fluxes estimated in the current work (1-3 mg cm^{-2} d^{-1}, at the high end), and assuming a munition material density[47] on the order of 2 g cm^{-3}, we can estimate that the surface of exposed underwater munitions will retreat at a rate on the order of 1 – 5 mm y^{-1}. This low value is consistent with observations in a study in Sweden where artillery shells were purposely cleaved and incubated in situ for three years, but very little dissolution was discernible by visual inspection[11]. This also explains why exposed munition material that was likely generated by low-order (i.e., incomplete) detonations in 2009[28] is still abundant at the Kolberger Heide study site. Indeed, 70 years have elapsed since most marine munitions were dumped following World War II, corresponding at the low range of our estimates to only about 13 cm of linear dissolution for munition material that was not enclosed in metal housings.

One striking result of the current study is the observation that solid munition material at this one study site appears to have a highly variable composition. There is a vast array of explosives formulations[43], and dumping activities likely included a variety of explosives types. As previous studies have noted, explosive formulation can affect dissolution behavior, with suppression of more soluble compounds such as TNT by less soluble components such as HMX[16,18–20]. Furthermore, explosive mixtures make underwater munitions point sources of a cocktail of different MC, and potential toxicological effects on associated ecosystems should be evaluated in the context of exposure to multiple toxicants.

The total release of toxic MC from underwater munitions depends on dissolution flux and the exposed surface area of explosive material, and this surface area is a critical factor for assessing risk of ecological exposure to MC. The total flux of MC to the water column depends on the exposed surface area, not the

number of munitions or area of the dump site. Constraining the area of exposed explosive surface is likely to be very difficult, especially given the first-order challenge of classifying munition-like objects on the seafloor[48]. Concentrations of dissolved MC in the water column may provide a more direct indication of the MC release rate, although loss by processes such as mixing, degradation/transformation, and sorption complicate the direct relationship. The variable but low dissolution fluxes estimated in the current work suggest that modeling of MC release and spread from underwater munitions would benefit from better constraint of the dissolution rate parameter, particularly under different mixing conditions. Solid explosives likely dissolve more rapidly in settings with high mixing rates, but may persist on the seafloor longer than expected under quiescent conditions. Where water mixing rates are low, concentrations of dissolved MC at the solid surface or within breached munitions can increase to levels that approach solubility limits. Given that underwater munitions can effectively act as bottom structure and habitat[9,10], marine organisms around the munitions may be exposed to concentrations many orders of magnitude higher than present in the bulk water column.

Acknowledgements

We greatly appreciate the enthusiastic sampling assistance from the Forschungstauchzentrum (Christian-Albrechts-Universität, Kiel) and the captain and crew of F/K Littorina. We also thank S. Sommer (GEOMAR) for his generous loan of the benthic chambers, and S. Cherednichenko for his instruction on their use. EMvdL wishes to thank Dr. Lars Umlauf for his idea of, and help with, using the law-of-the-wall. Two anonymous reviewers provided thoughtful and constructive comments that improved the manuscript. This work was funded by the German Federal Ministry of Education and Research (BMBF) through the project UDEMM (Umweltmonitoring für die DElaboration von Munition im Meer, Project number 03F0747, subprojects AkViCheMM and HyMeSiMM), and GEOMAR Helmholtz Centre for Ocean Research.

Supporting Information Available. Additional information on German-language references. Fig S1. Study site. Fig. S2. Water column profiles. Fig. S3. ADCP velocity profiles. Figure S4. Eddy diffusion coefficients calculated using the GETM model. Brief description of analyte sorption loss tests.

This information is available free of charge via the Internet at http://pubs.acs.org.

References

1. Carton, G. & Jagusiewicz, A. Historic Disposal of Munitions in U.S. and European Coastal Waters , How Historic Information Can be Used in Characterizing and Managing Risk. *Mar. Technol. Soc. J.* **43,** 16–32 (2011).

2. Monfils, R., Gilbert, T. & Nawadra, S. Sunken WWII shipwrecks of the Pacific and East Asia: The need for regional collaboration to address the potential marine pollution threat. *Ocean Coast. Manag.* **49,** 779–788 (2006).

3. Aker, J., Howard, B. & Reid, M. Risk Management For Unexploded Ordinance (UXO) In The Marine Environment. *Dalhousie J. Interdiscip. Manag.* **8,** 1–22 (2012).

4. Edwards, R. Danger from the deep. *New Sci.* **148,** 16–17 (1995).

5. Bohne, J. WWII bombs explode at North Sea wind farm. *Dtsch. Welle* (2012). at <http://www.dw.de/wwii-bombs-explode-at-north-sea-wind-farm/a-16360735>

6. Sanderson, H. & Fauser, P. Environmental Assessments Of Sea Dumped Chemical Warfare Agents: CWA report. *Sci. Rep. from DCE - Danish Cent. Environ. Energy* **174,** 1–116 (2015).

7. Tornero, V. & Hanke, G. Identification of marine chemical contaminants released from sea-based sources: A review focusing on regulatory aspects. *Eur. Comm. Jt. Res. Cent.* **JRC102452,** 1–130 (2016).

8. Lotufo, G. R., Chappell, M. A., Price, C. L., Ballentine, M. L., Fuentes, A. A., Bridges, T. D., George, R. D. & Glisch, E. Review and synthesis of evidence regarding environmental risks posed by munitions constituents (MC) in aquatic systems. *ERDC/EL TR-17-17.* 1–254 (2017).

9. Della Torre, C., Petochi, T., Corsi, I., Dinardo, M. M., Baroni, D., Alcaro, L., Focardi, S., Tursi, A.,

455 Marino, G., Frigeri, A. & Amato, E. DNA damage, severe organ lesions and high muscle levels of As
456 and Hg in two benthic fish species from a chemical warfare agent dumping site in the
457 Mediterranean Sea. *Sci. Total Environ.* **408,** 2136–2145 (2010).

458 10. McDonald, J. Demonstration of the Marine Towed Array on Bahia Salinas del Sur Vieques, Puerto
459 Rico. *ESTCP Rep. MM-0324.* 1–133 (2009).

460 11. Ek, H., Dave, G., Nilsson, E., Sturve, J. & Birgersson, G. Fate and effects of 2,4,6-trinitrotoluene
461 (TNT) from dumped ammunition in a field study with fish and invertebrates. *Arch. Environ.*
462 *Contam. Toxicol.* **51,** 244–252 (2006).

463 12. Porter, J. W., Barton, J. V. & Torres, C. Ecological, Radiological, and Toxicological Effects of Naval
464 Bombardment on the Coral Reefs of Isla de Vieques, Puerto Rico. *Warf. Ecol. A New Synth. Peace*
465 *Secur.* 65–122 (2011). doi:10.1007/978-94-007-1214-0

466 13. Koide, S., Silva, J. A. K., Dupra, V. & Edwards, M. Bioaccumulation of chemical warfare agents,
467 energetic materials, and metals in deep-sea shrimp from discarded military munitions sites off
468 Pearl Harbor. *Deep. Res. Part II Top. Stud. Oceanogr.* **128,** 53–62 (2016).

469 14. Strehse, J. S., Appel, D., Geist, C., Martin, H. J. & Maser, E. Biomonitoring of 2,4,6-trinitrotoluene
470 and degradation products in the marine environment with transplanted blue mussels (M. edulis).
471 *Toxicology* **390,** 117–123 (2017).

472 15. Lynch, J. C., Brannon, J. M. & Delfino, J. J. Dissolution rates of three high explosive compounds:
473 TNT, RDX, and HMX. *Chemosphere* **47,** 725–734 (2002).

474 16. Lynch, J. C., Myers, K. F., Brannon, J. M. & Delfino, J. J. Effects of pH and Temperature on the
475 Aqueous Solubility and Dissolution Rate of 2,4,6-Trinitrotoluene (TNT), Hexahydro-1,3,5-trinitro-
476 1,3,5-triazine (RDX), and Octahydro-1,3,5,7-tetranitro-1,3,5,7-tetrazocine (HMX). *J. Chem. Eng.*

Data **46,** 1549–1555 (2001).

17. Brannon, J. M., Price, C. B., Yost, S. L., Hayes, C. A. & Porter, B. E. Comparison of environmental fate and transport process descriptors of explosives in saline and freshwater systems. *Mar. Pollut. Bull.* **50,** 247–251 (2005).

18. Lever, J. H., Taylor, S., Perovich, L., Bjella, K. & Packer, B. Dissolution of composition B detonation residuals. *Environ. Sci. Technol.* **39,** 8803–8811 (2005).

19. Monteil-Rivera, F., Deschamps, S., Ampleman, G., Thiboutot, S. & Hawari, J. Dissolution of a new explosive formulation containing TNT and HMX: Comparison with octol. *J. Hazard. Mater.* **174,** 281–288 (2010).

20. Dontsova, K. M., Yost, S. L., Šimunek, J., Pennington, J. C. & Williford, C. W. Dissolution and Transport of TNT, RDX, and Composition B in Saturated Soil Columns. *J. Environ. Qual.* **35,** 2043–2054 (2006).

21. Thiboutot, S., Ampleman, G., Gagnon, A., Marois, A., Jenkins, T. F., Walsh, M. E., Thome, P. G. & Ranney, T. *Characterization Of Antitank Firing Ranges At CFB Valcartier, WATC Wainwright And CFAD Dundurn (DREV - R - 9809)*. (1998).

22. Fuller, M. E., Schaefer, C. E., Andaya, C. & Fallis, S. Production of particulate Composition B during simulated weathering of larger detonation residues. *J. Hazard. Mater.* **283,** 1–6 (2015).

23. Wang, P.-F., George, R. D., Wild, W. & Liao, Q. Defining Munition Constituent (MC) Source Terms in Aquatic Environments on DoD Ranges (ER-1453). Technical Report 1999 (2013).

24. Wang, P.-F., Liao, Q., George, R. & Wild, W. Release rate and transport of munitions constituents from breached shells in marine environment. *ACS Symp. Ser.* **1069,** 317–340 (2011).

498 25. Brannon, J. M. & Pennington, J. C. Environmental Fate and Transport Process Descriptors for
499 Explosives. *Strateg. Environ. Res. Dev. Progr. Install. Restor. Res. Progr. ERDC/ELTR-02-10* (2002).

500 26. Luning Prak, D. J. & O'Sullivan, D. W. Solubility of 2,4-Dinitrotoluene and 2,4,6-Trinitrotoluene in
501 Seawater. *J. Chem. Eng. Data* **51,** 448–450 (2006).

502 27. Frenz, U. Autonome Unterwasserfahrzeuge mit SAS-Technologie. *Lehre und Forsch.* **02-2014,** 11–
503 16 (2014).

504 28. Pfeiffer, F. *Bericht über die in-situ-Begleituntersuchungen zur Munitionssprengung in der Ostsee*
505 *vom 18.2.2009 (Ausschreibungsnummer: 4123-2009-41F)*. (2009). at <https://www.schleswig-
506 holstein.de/DE/Fachinhalte/M/meeresschutz/Downloads/Bericht_Begleituntersuchung_2009.pdf
507 ?__blob=publicationFile&v=1>

508 29. Pfeiffer, F. *Bericht über die in-situ-Begleituntersuchungen zur Munitionssprengung in der Ostsee*
509 *vom 28.2. – 18.3.2012 (Ausschreibungsnummer: ZB-U0-12-0027000-4121.6)*. (2012). at
510 <https://www.schleswig-
511 holstein.de/DE/Fachinhalte/M/meeresschutz/Downloads/Bericht_Heidkate.pdf?__blob=publicati
512 onFile&v=1>

513 30. Pfeiffer, F. Bericht über Zusammensetzung und Eigenschaften einer Schießwolleprobe
514 (Vergabenummer: ZB-50-14-0292000-4121.7). 1–26 (2014). at <https://www.schleswig-
515 holstein.de/DE/Fachinhalte/M/meeresschutz/Downloads/Bericht_Heidkate.pdf?__blob=publicati
516 onFile&v=1>

517 31. Szala, M. 2nd DAIMON Meeting Goslar, Germany 17-19th October 2016. (2016).

518 32. Radtke, H., Lipka, M., Bunke, D., Morys, C., Woelfel, J., Cahill, B., Böttcher, M. E., Forster, S., Leipe,
519 T., Rehder, G. & Neumann, T. Ecological ReGional Ocean Model with vertically resolved sediments

(ERGOM SED 1.0): coupling benthic and pelagic biogeochemistry of the south-western Baltic Sea. *Geosci. Model Dev.* **12,** 275–320 (2019).

33. Gledhill, M., Beck, A. J., Stamer, B., Schlosser, C. & Achterberg, E. P. Quantification of munition compounds in the marine environment by solid phase extraction – ultra high performance liquid chromatography with detection by electrospray ionisation – mass spectrometry. *Talanta* **200,** 366–372 (2019).

34. Schlosser, C., Streu, P., Frank, M., Lavik, G., Croot, P. L., Dengler, M. & Achterberg, E. P. H2S events in the Peruvian oxygen minimum zone facilitate enhanced dissolved Fe concentrations. *Sci. Rep.* **8,** 1–8 (2018).

35. Mohrholz, V., Naumann, M., Nausch, G., Krüger, S. & Gräwe, U. Fresh oxygen for the Baltic Sea - An exceptional saline inflow after a decade of stagnation. *J. Mar. Syst.* **148,** 152–166 (2015).

36. Gräwe, U., Friedland, R. & Burchard, H. The future of the western Baltic Sea: Two possible scenarios. *Ocean Dyn.* **63,** 901–921 (2013).

37. Klingbeil, K., Mohammadi-Aragh, M., Gräwe, U. & Burchard, H. Quantification of spurious dissipation and mixing - Discrete variance decay in a finite-Volume framework. *Ocean Model.* **81,** 49–64 (2014).

38. Thorpe, S. A. *The Turbulent Ocean*. (Cambridge University Press, 2005).

39. Holtermann, P. L., Umlauf, L., Tanhua, T., Schmale, O., Rehder, G. & Waniek, J. J. The Baltic Sea Tracer Release Experiment: 1. Mixing rates. *J. Geophys. Res. Ocean.* **117,** 1–18 (2012).

40. Rosen, G., Lotufo, G. R., George, R. D., Wild, B., Rabalais, L. K., Morrison, S. & Belden, J. B. Field validation of POCIS for monitoring at underwater munitions sites. *Environ. Toxicol. Chem.* **37,** 2257–2267 (2018).

41. Beck, A. J., Gledhill, M., Schlosser, C., Stamer, B., Böttcher, C., Sternheim, J., Greinert, J. & Achterberg, E. P. Spread, Behavior, and Ecosystem Consequences of Conventional Munitions Compounds in Coastal Marine Waters. *Front. Mar. Sci.* **5,** 1–26 (2018).

42. CRANK, J., McFARLANE, N. R., NEWBY, J. C., PATERSON, G. D. & PEDLEY, J. B. *Diffusion Processes in Environmental Systems*. (TRE MACMILLAN PRESS LTD, 1981). doi:10.1007/978-1-349-05825-9

43. Haas, R. & Thieme, J. Band 2 : Explosivstofflexikon. *Bestandsaufnahme von Rüstungsaltlastverdachtsstandorten der Bundesrepublik Deutschland, 2. Erweiterte Auflage, Umweltbundesamt [Inventory suspected armament Contam. sites Fed. Repub. Ger. Second Ext. Ed. Fed. Envi* 378 pp. (1996). at <https://www.umweltbundesamt.de/en/publikationen/bestandsaufnahme-von-1>

44. Morley, M. C., Yamamoto, H., Speitel, G. E. & Clausen, J. Dissolution kinetics of high explosives particles in a saturated sandy soil. *J. Contam. Hydrol.* **85,** 141–158 (2006).

45. Lynch, J. C. Dissolution Kinetics of High Explosive Compounds (TNT, RDX, HMX). *ERDC/EL Rep. TR-02-23.* 1–133 (2002).

46. Phelan, J. M., Romero, J. V, Barnett, J. L. & Parker, D. R. Solubility and dissolution kinetics of Composition B explosive in water. *Sandia Rep. SAND2002-2420.* 1–22 (2002).

47. Baytos, J. F. *LASL explosive property data (Vol. 4)*. (Univ of California Press, 1980).

48. Missiaen, T., Söderström, M., Popescu, I. & Vanninen, P. Evaluation of a chemical munition dumpsite in the Baltic Sea based on geophysical and chemical investigations. *Sci. Total Environ.* **408,** 3536–3553 (2010).